Chinese Chemical Letters 35 (2024) 109344

Contents lists available at ScienceDirect

Chinese Chemical Letters

journal homepage: www.elsevier.com/locate/cclet

A hydrogen-bonded organic framework containing fluorescent carbazole and responsive pyridyl units for sensing organic acids

Liangji Chen[1], Zhen Yuan[1], Fudong Feng, Xin Zhou, Zhile Xiong, Wuji Wei, Hao Zhang, Banglin Chen, Shengchang Xiang, Zhangjing Zhang*

Fujian Key Laboratory of Polymer Materials, College of Chemistry and Materials Science, Fujian Normal University, Fuzhou 350007, China

ARTICLE INFO

Article history:
Received 18 October 2023
Revised 14 November 2023
Accepted 27 November 2023
Available online 9 December 2023

Keywords:
Hydrogen-bonded organic framework
Organic acid sensing
Acids recognition
Carbazole luminescence
Pyridine protonation

ABSTRACT

Hydrogen-bonded organic frameworks (HOFs) are a promising candidate for optical sensing, but the lack of effective design strategies poses significant challenges to the construction of HOFs for organic acid sensing. In this work, the first HOF for organic acid sensing is reported by constructing a multiple-pyridine carbazole-based dense HOF, namely HOF-FJU-206, from a tripyridine-carbazole molecular 3,6-bis(pyridin-4-yl)-9-(4-(pyridin-4-yl)phenyl)-9*H*-carbazole (CPPY) with carbazole center for luminescence, pyridyl sites for its responsive of hydrogen proton, and narrow channels in the dense framework for the diffusion of hydrogen protons. HOF-FJU-206 exhibits differential responsively fluorescence sensing and recovery properties to formic, acetic, and propionic acids with different molecular sizes and pK_a value (acid dissociation constant). The dissociation degree of various acids can be determined by analyzing the slope of changes in both peak wavelength and intensity of *in-situ* fluorescence, which easily enables the dual-corrective recognition of different acids. The varying degree of protonation at pyridine sites is proved to be the reason for differential sensing of various acids, as demonstrated by ^{1}H NMR spectra, X-ray photoelectron spectroscopy (XPS) characterization, and modeling studies.

Hydrogen-bonded organic frameworks (HOFs) have provided an appealing and newly emerging class of crystalline materials as multifunctional resources for important applications such as gas separation, optical sensing, catalysis, electronics, and biomedicine [1–8]. High optical gain and various sensing functions can be easily achieved by rational design and select π-conjugated aromatic molecules with luminescent properties [9–12]. Meanwhile, the intrinsic flexibility hydrogen bonding enables HOFs easy to respond to external stimuli. By designing optical molecules with specific functional sites as organic monomer, HOFs are showing tremendous potential in optical sensing applications, such as sensing for explosives [13,14], aniline [15–17], acid vapors like HCl [18] and trifluoroacetic acid [19], medicine [20], metal ions [21,22] and temperature [23], as well as sensing devices like photoconduction [24,25], microlaser [26,27] and visualized separation column [28].

Organic acids such as formic acid (FA), acetic acid (AA), and propionic acid (PA) are widely used in medicine, agriculture, pharmaceuticals, foods and beverages, and other industries [29–33]. As one of the common harmful air pollutants, human exposure to their vapors will cause external chemical burns, while inhalation can lead to severe chemical pneumonitis, nerve injury, and dermatosis, and bring great damage for the environment [34–36]. The sensing detection of these monocarboxylic acids is essential but challenging due to their weak acidity than conventional inorganic acids, and most materials exhibit poor chemical stability upon exposure to organic acids. Only a few crystalline frameworks are reported [37–40] and an effective HOF-based sensor for detecting monocarboxylic acids has yet to be developed. It is crucial to develop an effective material design strategy for addressing this challenge.

Pyridine is an acid response functional group [41,42], and carbazole is a typical fluorescent material [43,44]. In this work, we propose a strategy for designing acid-sensing multifunctional crystalline materials through constructing the multiple-pyridine carbazole-based dense HOFs with carbazole center for luminescence, pyridyl sites for its responsive of hydrogen proton, and narrow channels in the dense framework for diffusion of hydrogen protons (Scheme 1). A tripyridine-carbazole molecular 3,6-bis(pyridin-4-yl)−9-(4-(pyridin-4-yl)phenyl)−9*H*-carbazole (CPPY) was designed and synthesized to construct the crystalline framework, namely HOF-FJU-206. HOF-FJU-206 exhibits efficient

* Corresponding author.
E-mail address: zzhang@fjnu.edu.cn (Z. Zhang).
[1] These authors contributed equally to this work.

https://doi.org/10.1016/j.cclet.2023.109344
1001-8417/

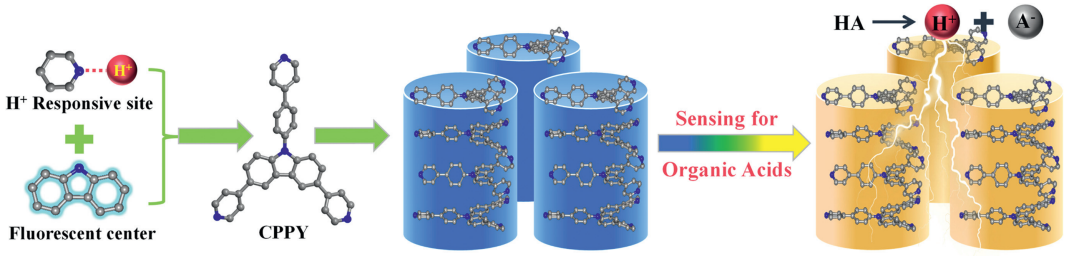

Scheme 1. The diagram of designing multiple-pyridine carbazole-based HOF with fluorescent carbazole center and H^+ responsive pyridyl site for sensing and distinguishing various organic acids.

responsive and distinguish for various monocarboxylic organic acids, which show differentiated luminescence controlled by different pK_a of various acids (pK_a is the acid dissociation constant that represents the ability of an acid to dissociate hydrogen ions. pK_a value: HCl (−7) > HNO_3 (−1.5) > HCOOH (3.7) > CH_3COOH (4.7) > C_2H_5COOH (4.8) [45–47]), as demonstrated by the *in-situ* fluorescence with changes in peak wavelength and intensity. Interestingly, the kinetic judgments of dual-corrective recognition for different acids can be achieved by utilizing the slope of the changes in peak wavelength and intensity of *in-situ* fluorescence. Furthermore, the protonation of pyridine sites by different acids entering the dense channels of HOF-FJU-206 was confirmed by ^{1}H NMR spectra, X-ray photoelectron spectroscopy (XPS) characterization, and modeling studies.

The novel HOF monomer CPPY was readily synthesized by Suzuki coupling reaction from 3,6-dibromo-9-(4-bromophenyl)−9*H*-carbazole and pyridine-4-boronic acid, and its molecular structure was confirmed by ^{1}H NMR spectroscopy (Figs. S1 and S2 in Supporting information). Block and colorless single crystals of HOF-FJU-206 that are suitable for single-crystal X-ray diffraction (SCXRD) studies can be obtained through simple recrystallization of CPPY from its DMF solution. The phase purity of the as-synthesized HOF-FJU-206 was confirmed by comparison of the experimental and simulated powder X-ray diffraction (PXRD) patterns (Fig. S3 in Supporting information). SCXRD analysis reveals that HOF-FJU-206 crystallizes in monoclinic system and cubic *P*2/c space group (Table S1 in Supporting information), showing a hydrogen bonded three-dimensional (3D) framework. In HOF-FJU-206, there are one complete CPPY molecule (red, linker 1) and two-half CPPY molecules (yellow, linker 2; blue, linker 3) in the asymmetric unit (Fig. 1a). Each linker 1 connects with four adjacent linkers through intermolecular C−H···N hydrogen bonds (with C···N distances of 3.490, 3.677 and 3.699 Å) to form a two-dimensional (2D) layer at the *bc* plane (Fig. 1b). Meanwhile, linker 2 connects with two adjacent linker 2 molecules through C62−H62···N8 hydrogen bonds (3.746 Å) to form a 1D chain, and linker 3 connects with each other to form another 1D chain with similar connection but hydrogen bonds distance of 3.734 Å, and further to give another 2D layer at the *bc* plane through C68−H68···N7 (3.636 Å) and C50−H50···N10 (3.675 Å) hydrogen bonds between the adjacent 1D chains (Fig. 1c). The layers are further connected with each other through multiple C−H···π interactions (Fig. 1d, with distances of 3.515–3.676 Å) and $\pi\cdots\pi$ interactions (with distances of 3.816-3.832 Å), giving a 3D framework stacked in an ABAB fashion (Figs. 1e and f). Interestingly, the distance range of the H-bonding interactions in HOF-FJU-206 is 3.4–3.8 Å, falling into the range of weak hydrogen bond [4], and is greater than the sum of Van der Waals radius of the C and N atoms, which allows for the diffusion of H protons into the dense channels and provides the driving force for acid vapor dissociation.

The acid response fluorescence sensing capability of HOF-FJU-206 was explored. As shown in Fig. 2a, the pristine HOF-FJU-206 shows blue fluorescence with a broad emission band maximum at 440 nm in the solid-state fluorescence spectrum under the UV excitation of 330 nm. After fumigation HOF-FJU-206 in HCOOH vapor for 0.5 h, the luminescence significantly changes to yellow with the fluorescence emission band center at 560 nm, indicating that HOF-FJU-206 can recognize and response to HCOOH vapor. In order to investigate the reversible of acid vapor recognition, the HCOOH-treated sample HOF-FJU-206-HCOOH was heated at 100 °C for 2 h. After heating, the sample backs to blue luminescence with fluorescence emission band at 456 nm, indicating that HOF-FJU-206 is sensitive to formic acid and its stimulated responsive property is reversible. Acetic acid showed a weaker effect for HOF-FJU-206 compared with formic acid, with the fluorescence emission peak shifted to 498 nm and almost recover to the initial fluorescence emission peak position (445 nm) after heating (Fig. 2b). Furthermore, propionic acid with larger pK_a value exhibits more slightly effect on the luminescence of HOF-FJU-206 (Fig. 2c).

In addition, we have investigated the sensing and reversible of the strongly acidic inorganic acids HCl and HNO_3 with smaller pK_a. The luminescence of HOF-FJU-206 significantly changes to yellow with the emission band center at 590 nm under HCl vapor, and the sample still shows yellow fluorescence with the fluorescence emission band slightly switched from 590 nm to 580 nm after heating (Fig. S4a in Supporting information), indicating the weak recovering of HOF-FJU-206-HCl. Due to the strong protonation capability, HNO_3 vapor show similar effect on HOF-FJU-206 compared with HCl (Fig. S4b in Supporting information). HOF-FJU-206 can recognize inorganic acids but cannot be efficiently recovered. This is due to the excessive acidity of strong inorganic acids, which leads to the overprotonation of HOF-FJU-206, making secondary dissociation challenging. The variation in sensing performance among different acids is linked to differences in their pK_a values. A lower pK_a corresponds to a faster dissociation rate of hydrogen ions, accelerating the protonation of pyridine within the HOF-FJU-206 framework. These findings demonstrate that HOF-FJU-206 can recognize not only organic acids of formic, acetic, and propionic acids, but also inorganic acids of HCl and HNO_3. The differential in luminescence and recovery properties also enables HOF-FJU-206 the efficient distinguish of organic and inorganic acids, and organic acids of formic, acetic and propionic acids with different pK_a value. Additionally, the PXRD patterns of the samples treated with HCl and HNO_3 were significantly widened and no longer sharp (Fig. S5 in Supporting information), indicating that the high protonation degree of the strong acidic inorganic acids on pyridine sites leads to the destruction of the crystalline framework. In comparison, HOF-FJU-206 still maintains its crystallinity after the treatment of formic acid, acetic acid, or propionic acid vapors.

The fluorescence signal of HOF-FJU-206 after fumigation with different concentrations of acid vapors was characterized to investigate the effect of acid concentration on its fluorescence properties. As shown in Fig. 2d, the relative fluorescence shift of HOF-FJU-206 gradually increased with increasing HCOOH concentration, the relative displacement shows a linear variation under the HCOOH atmosphere of 0–2 mol/L ($y = 56.32x + 0.336$, $R^2 = 0.977$). The limit

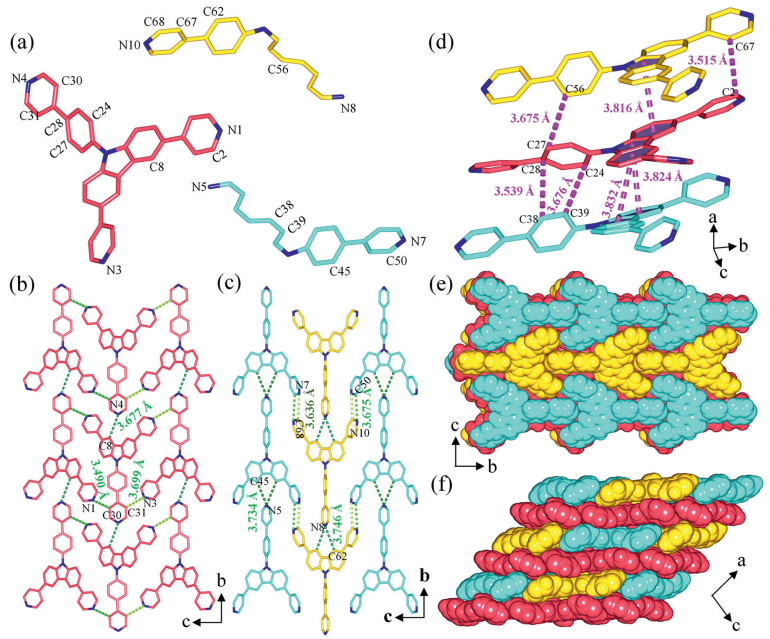

Fig. 1. Crystal structure of HOF-FJU-206. (a) Three CPPY molecules in the asymmetric unit. Red, linker 1; Yellow, linker 2; Blue, linker 3. H atoms are omitted for clarity. (b) The 2D molecular layer self-assembled by linker 1. (c) Another 2D layer formed by linker 2 and linker 3. (d) Interactions between the layers. The formed 3D framework of HOF-FJU-206 along (e) *a* axis and (f) *b* axis.

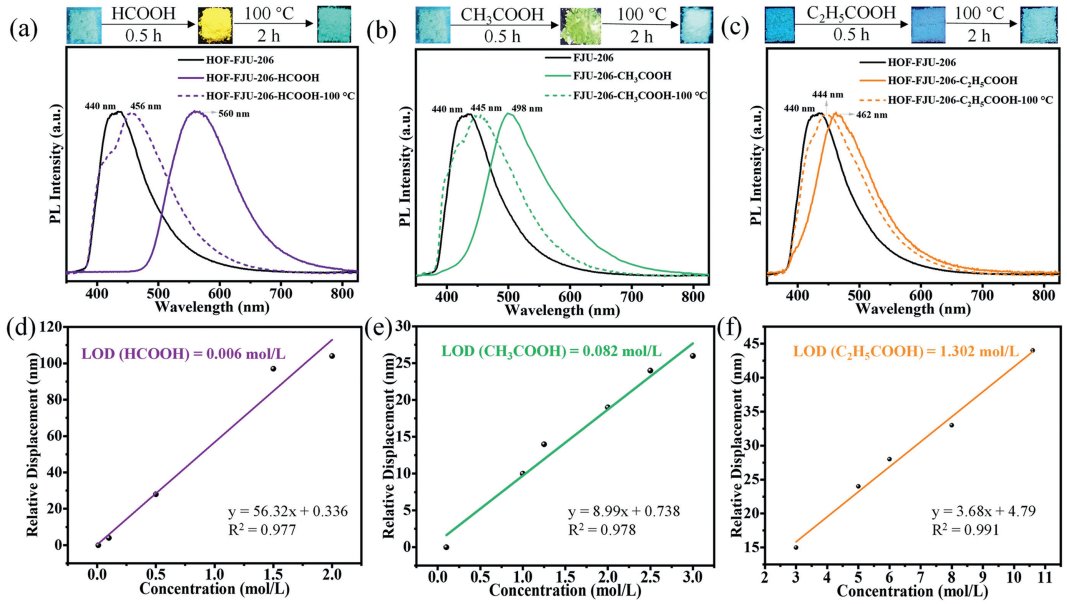

Fig. 2. Fluorescence emission pattern (under 330 nm excitation) of HOF-FJU-206 before and after the fumigation in (a) formic acid, (b) acetic acid, (c) propionic acid vapors for 0.5 h and then heating at 100 °C for 2 h. The LOD and linear correlation between acid concentration and fluorescence shift for (d) formic acid, (e) acetic acid and (f) propionic acid.

of detection (LOD) of HOF-FJU-206 for HCOOH was 0.006 mol/L according to the standard working curve. Acetic acid shows the linear variation within the concentration range of 0–3 mol/L, with a LOD of 0.082 mol/L (Fig. 2e). The LOD of HOF-FJU-206 for propionic acid is 1.302 mol/L within the concentration of 2–11 mol/L (Fig. 2f). In comparison, HOF-FJU-206 exhibits weaker LOD for HCl and HNO_3, which may be due to the structure destruction of HOF-FJU-206 by the strongly acidic inorganic acids (Figs. S4c and d in Supporting information). The above results confirmed that HOF-FJU-206 may be a promising material for acid sensing and can be applicable for the sensing detection of low concentration organic acid vapors.

The *in-situ* time-dependent emission spectra were recorded in a self-designed testing device to further explore the sensing process of acid vapors (Fig. S6 in Supporting information). After injecting HCOOH to the sample cell with HOF-FJU-206, the original emission band around 440 nm continuously decreases in intensity and gradual movement towards longer-wavelength, and the original band completely disappeared at 3.75 min (Fig. 3a). Meanwhile, a new band appears around 580 nm at 4 min and the intensity gradually increases progressively and reaches its highest peak at 30 min. Commission Internationale d'Eclairage (CIE) chromatogram obtained with the fluorescence spectral data demonstrated the fluorescence change from blue to yellow of HOF-FJU-206 in HCOOH vapor, which offers the possibility of visual sensing through fluorescent color (the inset in Fig. 3a). The other acid vapors show the similar fluorescence changes over time, but accompanied with dif-

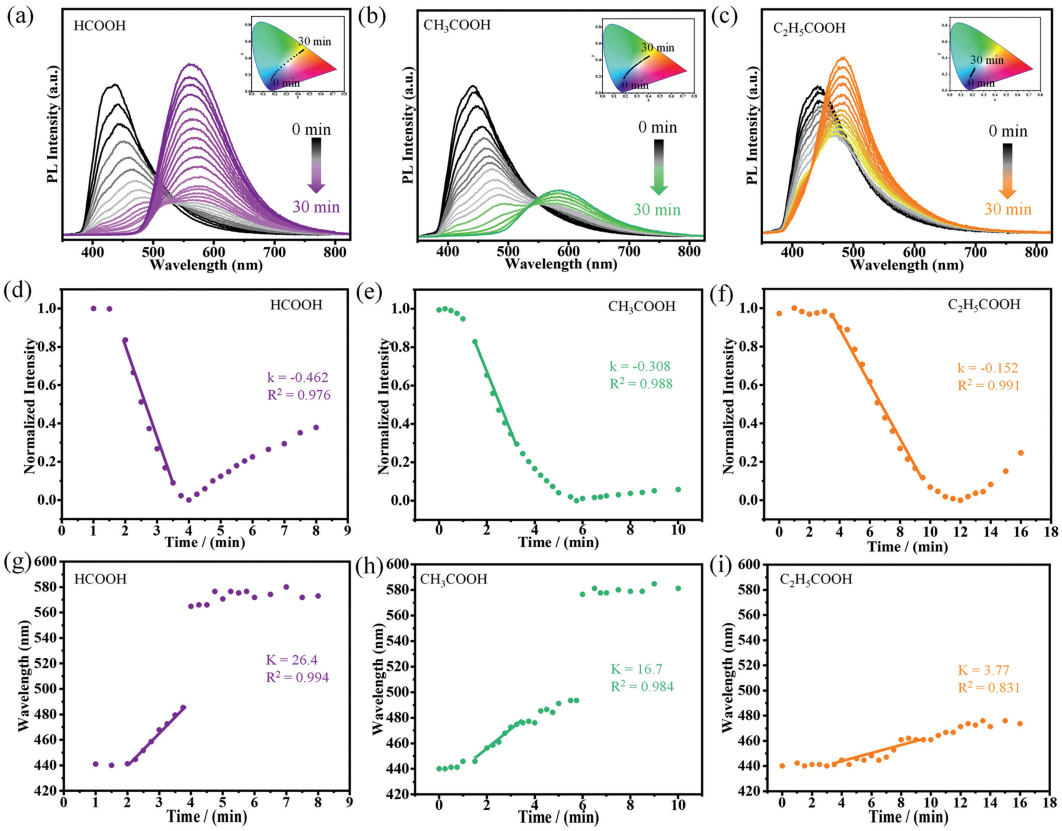

Fig. 3. Time-dependent emission spectra of HOF-FJU-206 under the fumigation of acid vapors: (a) Formic acid, (b) acetic acid and (c) propionic acid. The insets are the CIE chromaticity diagram for showing the color variation of HOF-FJU-206 with the diffusion time of acid vapors. The time-dependent change of (d-f) intensity and (g-i) wavelength of the highest fluorescence peak in the emission spectra of HOF-FJU-206 for various acid vapors.

ferential response rate. The original peak of HOF-FJU-206 in acetic acid vapor completely disappeared at 5.75 min and the new emission peak centered at 580 nm appeared at 6 min (Fig. 3b). The disappearance of the original peak in propionic acid occurs at 7 min, while the appearance of new emission peaks is at 8 min (Fig. 3c). The differential response rate of various acid vapors may be due to the different dissociation rates of HOF-FJU-206 upon different acids.

The time-dependent wavelength and intensity change was investigated to further explore the dissociation rate of various acid vapors in HOF-FJU-206. As shown in Figs. 3d and g, the fluorescence peak intensity and wavelength almost not change within 2 min after injecting HCOOH vapor, which corresponds to the dissociation and diffusion process of formic acid vapor in the test chamber at room temperature. Subsequently, the intensity of the fluorescence peak sharply decreases, accompanied by a shift in wavelength towards the longer wavelength direction. The slope of the decrease in fluorescence intensity is −0.4625, and the slope of the wavelength change is 26.4, representing the responsive rate of hydrogen protons dissociated from formic acid within the framework. The variation pattern of the intensity and wavelength of the maximum fluorescence peak is consistent as formic acid > acetic acid > propionic acid (Figs. 3d–i), indicating that formic acid has the fastest responsive rate on the HOF-FJU-206 framework, followed by acetic acid, and propionic acid is the slowest. In addition, the slopes of HCl and HNO_3 are subdued (Fig. S7 in Supporting information), which may be due to the stronger acidic inorganic acids disrupting the framework structure of HOF-FJU-206. The above results indicate that acids with different pK_a have different responsive rates, and therefore resulting in differential sensing ability of HOF-FJU-206 towards different acids. Therefore, the differential fluorescence peak and wavelength change trend can provide dual correction function for sensing different acids (Fig. S8 in Supporting information).

The acid vapor induced fluorescence change of HOF-FJU-206 may be attributed to the protonation effect of acid dissociated hydrogen protons on pyridine groups from the framework. The single-crystal data of samples following acids fumigation exhibited no pronounced alterations at the level of individual monomeric molecular entities; instead, a slight expansion in unit cell volume was observed (Table S1 in Supporting information). This phenomenon could be ascribed to the penetration of acidic species into the crystal lattice, albeit with relatively disordered protonation of hydrogen species. To further study the protonation on pyridine, we tested the ^{1}H NMR data of HOF-FJU-206 and its samples fumigated in different acid vapors. The samples are dissolved in deuterated DMSO solvent for the ^{1}H NMR testing. As shown in Fig. 4a, there are 22 hydrogen atoms in the monomer molecule CPPY in the HOF-FJU-206 framework, and their chemical shifts are 8.99, 8.71, 8.68, 8.16, 8.00, 7.88 and 7.60 ppm. The ^{1}H NMR peaks of pristine HOF-FJU-206 are correspond to the chemical shift of H atoms at various positions (Fig. 4b). The chemical shifts of all H atoms in the sample after fumigation with HCl show significant changes (Fig. S9a in Supporting information), which may be due to the adsorption of Cl^- on the HOF-FJU-206 framework affect the chemical environment of H [48]. Interestingly, HOF-FJU-206 exhibits noteworthy alterations following treatment with HNO_3. The peaks originally positioned at 8.99, 8.71, 8.68, 8.00, and 7.88 ppm have shifted to 9.04, 8.74, 8.04, and 8.02 ppm, respectively (Fig. S9a), which are correspond to the H atoms on the pyridine group and the adjacent H on carbazole of CPPY. This highlights that nitric acid fumigation induces shifts in the chemical environment of hydrogen atoms

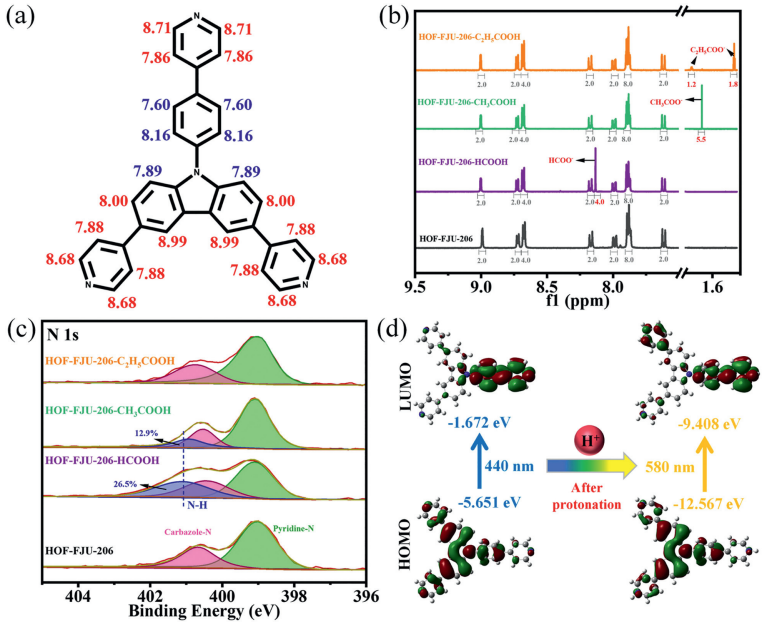

Fig. 4. (a) Chemical shift of hydrogen atom on monomer molecule CPPY. (b) ^{1}H NMR spectra in DMSO–d_6, XPS spectra (c) of HOF-FJU-206 and the acid vapors fumigated samples. (d) The frontier molecular orbitals of CPPY and CPPY@H^{+}.

on pyridine and adjacent carbazole units. This observation robustly supports the protonation of acid vapor on the pyridine sites within the HOF-FJU-206 framework. However, given that nitrate ions lack extra hydrogen atoms, quantifying the extent of nitric acid protonation on individual CPPY molecules within HOF-FJU-206 is difficult.

In comparison, the chemical shift of H atom of CPPY did not change obviously after fumigation with organic acids (Fig. 4b), which may be because the protonation ability of organic acids with higher pK_a value is weaker than inorganic acids and no damage to the framework structure. However, we found a new nuclear magnetic peak at 8.13 ppm in the formic acid treated sample, which corresponds to formic acid ions $HCOO^{-}$. The integral area shows that there are four H atoms, indicating that four formic acid molecules participate in the protonation for each CPPY molecule. Similarly, HOF-FJU-206-CH_3COOH shows an acetate ion NMR peak at 1.90 ppm, and its integral area (5.5) exhibits that 1.8 acetic acid molecules are involved in the protonation for each CPPY molecule. Due to the weak protonation ability of propionic acid molecules with largest pK_a, only 0.6 (based on each CPPY molecule) trace propionate ions were detected, with their positions at 0.98 and 2.21 ppm. This indicates that these organic acids have different degrees of dissociation and protonation on the pyridine site in the framework: formic acid > acetic acid > propionic acid.

XPS characterization was employed to further verify the protonation of HOF-FJU-206 by different acid vapors. As shown in Fig. 4c, the N 1s spectrum of HOF-FJU-206 show peaks centered at 400.7 and 399.1 eV, which are attributed to the N atoms from pyridine and carbazole, respectively. After fumigation with HCOOH, a new peak with an area ratio of 26.5% appeared at 401.2 eV, which belongs to the N–H on the protonation pyridine. This indicates that pyridine in HOF-FJU-206 is partially protonation. The N–H peak ratio of the acetic acid fumigated sample is 12.9%, while that of propionic acid is difficult to find. Different N–H peak areas mean that these acids have differential protonation capability, and the protonation degrees are HCOOH > CH_3COOH > CH_3CH_2COOH, consistent with the ^{1}H NMR data. The samples fumigated with HCl and HNO_3 show strong N–H peaks with ratio of 50.7% and 43.2%, respectively, indicating their strong protonation ability to HOF-FJU-206 (Fig. S9b in Supporting information). In addition, HOF-FJU-206-HNO_3 shows extra N-H and N-O and N=O peaks at 408.0 eV and 406.4 eV, which is attributed to HNO_3 adsorbed on the surface of HOF-FJU-206.

In order to further prove the dissociation of hydrogen proton from various acids into the framework, thermogravimetric (TG) curves of samples treated with different acid vapors were tested. As shown in Fig. S10a (Supporting information), HOF-FJU-206 has no decomposition of the mass until 406 °C due to the absence of additional guests. Comparatively, HOF-FJU-206-HCOOH shows obvious weight loss of 34.4% before 147 °C. This indicates that bulk protonic hydrogen is adsorbed into the framework and binding with pyridine. The weight loss of HOF-FJU-206-CH_3COOH is 11%, while that of propionic acid is almost the same as that of the original sample. The weight loss of HCl and HNO_3 fumigated sample are 33% and 10%, respectively (Fig. S10b in Supporting information), indicating that their dissociated protonic hydrogen can also enter the framework. The above results demonstrate that the different dissociate rate of organic acids with different pK_a result in different amount of hydrogen protons entering the framework and lead to differentiated protonation degree for the difference of luminescence.

Density functional theory calculations were applied to the original and protonated molecules to gain in-depth study of the relationship between the fluorescence change and the protonation process of CPPY (Fig. 4d). The highest occupied molecular orbital (HOMO) of CPPY mainly concentrates on the carbazole group and two pyridine groups attached to the benzene ring on the carbazole, whereas the lowest unoccupied molecular orbital (LUMO) mainly consists the benzene ring and pyridine groups connected to the nitrogen on carbazole. Similarly, the distribution of HOMO and LUMO was almost not changed after the protonation of the three pyridine sites in CPPY (CPPY@H^{+}), but the energy of both HOMO and LUMO for CPPY@H^{+} are significantly reduced. Compared to HOMO, LUMO is reduced more and results in a reduction of the energy gap of CPPY@H^{+}, and the energy gap reduction from 3.979 eV to 3.159 eV after protonation. This indicates that protonation can greatly reduce the energy gap and short down the energy gap difference of CPPY in the framework, and the smaller energy gap resulted in the

fluorescence redshift. Based on the above results, the degree of dissociation of acids with varying pK_a values differed on the HOF-FJU-206 framework, resulting in diverse quantities of hydrogen protons penetrating the framework. Consequently, this led to distinct levels of pyridine protonation on the framework, thereby inducing variations in luminescence.

In summary, we have reported the first HOF for organic acids sensing by constructing a multiple-pyridine carbazole-based dense structure with carbazole center for luminescence, pyridyl sites for its responsive of hydrogen proton, and narrow channels in the dense framework for the diffusion of hydrogen protons. Due to the varying dissociation degrees of acidic vapors with different pK_a values on the HOF-FJU-206 framework, HOF-FJU-206 can exhibit differential sensing outcomes towards different acids, including differences in luminescence color, fluorescence peak intensity and wavelength, and recovery property. Interestingly, we can also achieve dual-corrective recognition of different acids by utilizing the slope of the changes in peak wavelength and intensity of *in-situ* fluorescence. We have demonstrated that the differential protonation degree at pyridine sites in dense framework through pK_a is an effective strategy for achieving fluorescence sensing, we believe this work will pave the way for the development of advanced HOFs with a diverse array of stimulus-responsive functionalities.

Declaration of competing interest

The authors declare that they have no known competing financial interests or personal relationships that could have appeared to influence the work reported in this paper.

Acknowledgments

This work was financially supported by the National Natural Science Foundation of China (Nos. 22271046, 21971038, 21975044), the Fujian Provincial Department of Science and Technology (No. 2019L3004), and the Foundation of National Key Laboratory of Human Factors Engineering (No. HFNKL2023W04).

Supplementary materials

Supplementary material associated with this article can be found, in the online version, at doi:10.1016/j.cclet.2023.109344.

References

[1] B. Wang, R.B. Lin, Z. Zhang, S. Xiang, B. Chen, J. Am. Chem. Soc. 142 (2020) 14399–14416.
[2] Z. Zhang, Y. Ye, S. Xiang, B. Chen, Acc. Chem. Res. 55 (2022) 3752–3766.
[3] Z.J. Lin, S.A.R. Mahammed, T.F. Liu, R. Cao, ACS Cent. Sci. 8 (2022) 1589–1608.
[4] R.B. Lin, Y. He, P. Li, et al., Chem. Soc. Rev. 48 (2019) 1362–1389.
[5] R.B. Lin, B. Chen, Chem 8 (2022) 2114–2135.
[6] S.C. Pal, D. Mukherjee, R. Sahoo, S. Mondal, M.C. Das, ACS Energy Lett. 6 (2021) 4431–4453.
[7] Z. Yuan, X. Jiang, L. Chen, et al., CCS Chem. 6 (2024) 663–671.
[8] Z. Yuan, L. Chen, X. Zhou, et al., J. Mater. Chem. A 11 (2023) 21857–21863.
[9] M.R.d. Nunzio, I. Hisaki, A. Douhal, J. Photochem. Photobiol. C (2021) 100418.
[10] S. Cai, H. Shi, Z. Zhang, et al., Angew. Chem. Int. Ed. 57 (2018) 4005–4009.
[11] S. Chen, Y. Ju, H. Zhang, et al., Angew. Chem. Int. Ed. (2023) e202308418.
[12] Q. Huang, X. Chen, W. Li, et al., Chem 9 (2023) 1241–1254.
[13] Z. Sun, Y. Li, L. Chen, X. Jing, Z. Xie, Cryst. Growth Des. 15 (2015) 542–545.
[14] C. Zhang, F. Sun, Y. He, ACS Appl. Mater. Interfaces 15 (2023) 9970–9977.
[15] B. Wang, R. He, L.H. Xie, et al., J. Am. Chem. Soc. 142 (2020) 12478–12485.
[16] Z. Ke, K. Chen, Z. Li, et al., Chin. Chem. Lett. 32 (2021) 3109–3112.
[17] Z. Fan, S. Zheng, H. Zhang, et al., Chin. Chem. Lett. 33 (2022) 4317–4320.
[18] E. Gomez, Y. Suzuki, I. Hisaki, M. Moreno, A. Douhal, J. Mater. Chem. C 7 (2019) 10818–10832.
[19] G. Xia, Z. Jiang, S. Shen, et al., Adv. Opt. Mater. 7 (2019) 1801549.
[20] Q. Yin, P. Zhao, R.J. Sa, R. Cao, et al., Angew. Chem. Int. Ed. 57 (2018) 7691–7696.
[21] H. Zhou, Q. Ye, X. Wu, et al., J. Mater. Chem. C 3 (2015) 11874–11880.
[22] H. Wang, Z. Bao, H. Wu, et al., Chem. Commun. 53 (2017) 11150–11153.
[23] J.F. Feng, X.Y. Yan, Z.Y. Ji, T.F. Liu, R. Cao, ACS Appl. Mater. Interfaces 12 (2020) 29854–29860.
[24] X. Zheng, N. Xiao, Z. Long, et al., Synth. Met. 263 (2020) 116365.
[25] Y. Suzuki, N. Tohnai, A. Saeki, I. Hisaki, Chem. Commun. 56 (2020) 13369–13372.
[26] Y. Lv, D. Li, A. Ren, et al., ACS Appl. Mater. Interfaces 13 (2021) 28662–28667.
[27] Y. Lv, Z. Xiong, Y. Li, et al., J. Phys. Chem. Lett. 13 (2022) 130–135.
[28] L. Chen, Z. Yuan, H. Zhang, et al., Angew. Chem. Int. Ed. 61 (2022) e202213959.
[29] A. Duscha, B. Gisevius, S. Hirschberg, et al., Cell 180 (2020) 1067–1080.e16.
[30] D. Mellmann, P. Sponholz, H. Junge, M. Beller, Chem. Soc. Rev. 45 (2016) 3954–3988.
[31] W. Zhang, F. Zhang, Y.X. Li, R.J. Zeng, Bioresour. Technol. 272 (2019) 458–464.
[32] Y. Yin, W. Song, J. Wang, Bioresour. Technol. 364 (2022) 128074.
[33] K.M. Lynch, E. Zannini, S. Wilkinson, L. Daenen, E.K. Arendt, Compr. Rev. Food Sci. Food Saf. 18 (2019) 587–625.
[34] M.E. Genovese, A. Athanassiou, D. Fragouli, J. Mater. Chem. A 3 (2015) 22441–22447.
[35] N.L. Torad, H. El-Hosainy, M. Esmat, et al., ACS Appl. Mater. Interfaces 13 (2021) 48595–48610.
[36] Y. Zhang, J. Liu, X. Chu, S. Liang, L. Kong, J. Alloys Compd. 832 (2020) 153355.
[37] R.L. Liu, W.T. Qu, B.H. Dou, Z.F. Li, G. Li, Chem. Asian J. 15 (2020) 182–190.
[38] R.L. Liu, Z.Q. Shi, X.Y. Wang, Z.F. Li, G. Li, Chem. Eur. J. 25 (2019) 14108–14116.
[39] M. Liu, J. Zhang, Y.R. Kong, et al., ACS Mater. Lett. 3 (2021) 1746–1751.
[40] Z. Wei, J. Song, R. Ma, K. Ariga, L.K. Shrestha, Chemosensors 10 (2022) 16.
[41] J.B. Arockiam, S. Ayyanar, Sensor. Actuat. B: Chem. 242 (2017) 535–544.
[42] A.E. Bejan, M.D. Damaceanu, Synth. Met. 268 (2020) 116498.
[43] J.X. Wang, Y.G. Fang, C.X. Li, et al., Angew. Chem. Int. Ed. 59 (2020) 10032–10036.
[44] X.J. Kong, X. Ji, T. He, et al., ACS Appl. Mater. Interfaces 12 (2020) 35375–35384.
[45] Y.R. Shin, I.Y. Jeon, J.B. Baek, Carbon 50 (2012) 1465–1476.
[46] C.X. Jiang, J.H. Di, C. Su, et al., Bioresour. Technol. 268 (2018) 315–322.
[47] J.E. Jeong, I.A. Cho, C.Y. Lee, Fuel 336 (2023) 126859.
[48] G. Baggi, M. Boiocchi, C. Ciarrocchi, L. Fabbrizzi, Inorg. Chem. 52 (2013) 5273–5283.